BOREAS An international journal of Quaternary research

Timing and flow pattern of the Orta Glacier (European Alps) during the Last Glacial Maximum

JOCHEM BRAAKHEKKE, SUSAN IVY-OCHS, GIOVANNI MONEGATO, FRANCO GIANOTTI, SILVANA MARTIN, STEFANO CASALE AND MARCUS CHRISTL

BOREAS

Braakhekke, J., Ivy-Ochs, S., Monegato, G., Gianotti, F., Martin, S., Casale, S. & Christl, M.: Timing and flow pattern of the Orta Glacier (European Alps) during the Last Glacial Maximum. *Boreas*. https://doi.org/10.1111/bor.12427. ISSN 0300-9483.

Knowledge of the glacial chronologies for the Last Glacial Maximum (LGM) helps in understanding the interactions between climate, topography and glacier development. In this sense, the investigation of the Lake Orta moraine amphitheatre (Alpine foreland, northern Italy) allowed spatial and temporal reconstruction of the Orta Glacier. The end-moraine system was investigated by means of geomorphological field surveys, analysis of 13 rock samples for cosmogenic ^{10}Be and ^{36}Cl concentrations, and remote sensing analysis. The dating results indicate that the age of the outer moraine belt is concordant with the LGM culmination at 26.5–23 ka, as found in other amphitheatres in the Alps. This new age estimate of the outermost moraines shows that the maximum extent of the Orta Glacier during the LGM was significantly bigger than recently suggested. A younger stabilization phase of the glacier front at about 19 ka indicates that the onset of the withdrawal of glaciers from the lower Alpine valleys started later. Provenance analysis of the boulders shows that the greatest contribution of ice to the Orta Glacier came from the Anzasca Valley rather than the major Ossola Valley. This reflects the closeness (about 45 km) to the foreland of the high-elevated accumulation area of the Monte Rosa massif (4634 m a.s.l.), whose eastern glacier seems to have reached the lower valley faster than the trunk Toce Glacier. This fact underlines the key role played by high-elevation accumulation areas that are located close to the foreland in controlling the path and geometry of major glaciers in the Alps.

Jochem Braakhekke, Department of Earth Sciences, ETH Zurich, Zurich 8092, Switzerland; Susan Ivy-Ochs, Department of Earth Sciences, ETH Zurich, Zurich 8092, Switzerland and Laboratory of Ion Beam Physics, ETH Zurich, Otto-Stern-Weg 5, Zurich 8093, Switzerland; Giovanni Monegato (corresponding author: giovanni.monegato@igg.cnr.it), Institute of Geosciences and Earth Resources National Research Council, Via Gradenigo 6, Padova (PD) 35131, Italy; Franco Gianotti, Dipartimento di Scienze della Terra, Università di Torino, Via Valperga Caluso 35, Torino 10125, Italy; Silvana Martin, Dipartimento di Geoscienze, Università di Padova, Via Gradenigo 6, Padova (PD) 35131, Italy; Stefano Casale and Marcus Christl, Laboratory of Ion Beam Physics, ETH Zurich, Otto-Stern-Weg 5, Zurich 8093, Switzerland; *received 12th April 2019, accepted 20th November 2019.*

During the Late Pleistocene cold phases, the European Alps hosted large glacier systems whose chronologies have been continuously updated (Preusser 2004; Ivy-Ochs *et al.* 2008; Heiri *et al.* 2014; Ivy-Ochs 2015; Monegato & Ravazzi 2018). From this perspective, the history of the Alpine glaciers during the Last Glacial Maximum (LGM, 26.5–19 ka according to Clark *et al.* 2009 or 30–16.5 ka after Lambeck *et al.* 2014) has been assessed through stratigraphical and geomorphological studies in many Alpine end-moraine systems, which yielded new chronological constraints for the maximum ice extents (Jorda *et al.* 2000; Monegato *et al.* 2007, 2017; Gianotti *et al.* 2008, 2015; Akçar *et al.* 2011; Preusser *et al.* 2011; Ravazzi *et al.* 2012; Reber *et al.* 2014; Salcher *et al.* 2015; Federici *et al.* 2017; Ivy-Ochs *et al.* 2018) and deglaciation phases (Fontana *et al.* 2014; Ravazzi *et al.* 2014; Scapozza *et al.* 2014; Reitner *et al.* 2016; Wirsig *et al.* 2016). On the other hand, remarkable differences in glacier development and size exist between the northern and western sectors of the Alps, where large piedmont lobes spread onto the forelands, and the glaciers on the eastern and southern sides, where glaciers for the most part remained confined within the valleys (Fig. 1A; Ehlers & Gibbard 2004). A better comprehension of the development and withdrawal of an Alpine glacier, including ice-flow patterns, has come from recent modelling of the LGM Rhine Glacier (Jouvet *et al.* 2017; Cohen *et al.* 2018). These results underline how integrating chronology and erratic boulder provenance can help in deciphering how fast the Alpine glaciers grew at the LGM onset.

The development of models reconstructing climate (e.g. Beghin *et al.* 2015; Luetscher *et al.* 2015) and glaciers (Becker *et al.* 2016; Seguinot *et al.* 2018) provide visualization of how the glacier advances may have taken place, but these models need reliable chronological and field constraints. In the Alps, many sectors still require detailed studies for constraining the chronology of the LGM, including the central southern Alps (Fig. 1A). Here large end-moraine systems, also called moraine amphitheatres (Fairbridge 1968), are the results of multiple glaciations and fluctuations of the large Toce-Ticino and Adda Glacier systems (Penck & Brückner 1901–1909; Jäckli 1970; Bini *et al.* 2004, 2014). Chronological constraints (radiocarbon dating and biological proxies) are scarce and the few data available are mostly related to the Lateglacial (see Scapozza *et al.* 2014 for a synthesis). The present study is focused on the Orta moraine amphitheatre, which encircles Lake Orta in north Italy and portrays part of the major Toce-Ticino Glacier lobe.

During the LGM, the Orta Glacier was a lobe that flowed off the Toce Glacier to the south at Gravellona

DOI 10.1111/bor.12427

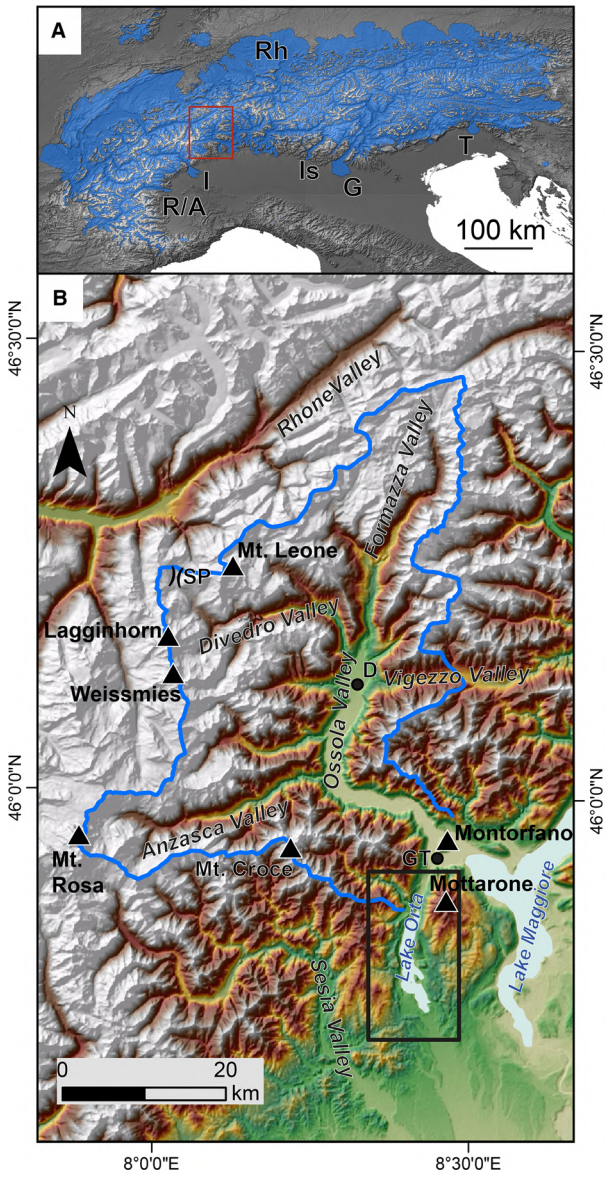

Fig. 1. A. Map of the Alpine ice-extent during the LGM (Ehlers & Gibbard 2004); study area in the red box, labelled end-moraine systems are: G = Garda; I = Ivrea; Is = Iseo; Rh = Rhine; R/A = Rivoli/Avigliana; T = Tagliamento. B. Outline of Toce River catchment (blue line indicates the watershed); study area of Fig. 3 in black box. D = Domodossola; GT = Gravellona Toce; SP = Simplon Pass.

Toce (Fig. 1B). The Toce Glacier catchment is very asymmetric with a high elevated western sector with accumulation areas above 4000 m a.s.l. from where large tributary glaciers flowed down the Anzasca Valley (Monte Rosa accumulation area) and the Divedro Valley (Weissmeiss-Lagginhorn accumulation area). In contrast, the eastern tributary valleys reach their highest elevations at about 2600 m a.s.l., with some northern peaks reaching 3000 m a.s.l. (Formazza Valley). In the middle Ossola Valley another junction with the Ticino glacier occurred along the tributary Vigezzo Valley, located along the Centovalli Fault (Fig. 2). In addition, the Toce Glacier likely received contributions from the Rhône ice dome through the transfluence at Simplon Pass (Florineth & Schlüchter 1998; Kelly *et al.* 2004). The major outlet of the Toce Glacier catchment was the Ossola Valley, where it merged with the large tributary glacier flowing down the eastern side of Monte Rosa along the Anzasca Valley. Due to the absence of a right lateral confining valley wall, the Toce Glacier diverged at the isolated granite hill of Montorfano (Fig. 1B) into one lobe that went south into the Orta Valley and another, the main branch, that continued to the southeast into the Lake Maggiore basin, where it merged with the Ticino Glacier.

Based solely on geomorphological observations and associated interpreted age assignments but with no chronological constraints, several divergent interpretations of the extent of the LGM glacier in the Orta Valley have been proposed (Penck & Brückner 1901–1909; Novarese 1927; Sacco 1930; Castiglioni 1940; Jäckli 1970; Hantke 1983; Vai & Cantelli 2004; Bini *et al.* 2009). Earlier authors favoured the greater extent, while more recent authors suggested a much smaller extent for the LGM (Fig. 3A). We aim at disentangling the age interpretation through chronologically constraining the moraines related to the LGM. The age assessment of the Orta end-moraine system allows discussions of the development of the Orta Glacier in the setting of the Alpine LGM and suggests how high-elevation accumulation areas located close to the foreland affected the flow of the ice streams.

Study area

Geological and geomorphological setting

The bedrock of the Toce mountain basin (Fig. 2, Table 1) can be subdivided into: (i) the South Alpine domain including a Palaeozoic basement lacking Alpine metamorphism, and (ii) the North Alpine domain characterized by a stack of basement and cover nappes with high-pressure Alpine metamorphism of Cretaceous age, overprinted by greenschist to amphibolite facies metamorphism of Cenozoic age (Lepontine Dome: Frey *et al.* 1999; Oberhänsli *et al.* 2004). The latter includes the Helvetic nappes, the Penninic nappes and the Sesia-Lanzo Zone (SL). The Canavese Zone (ZC), which crops out within the two branches of the Canavese Fault, is a tectonic slice zone (Piana *et al.* 2017) characterized by a greenschist Alpine metamorphism. The Canavese Fault is the southwestern continuation of the Periadriatic/Insubric lineament separating the North and South Alpine domains. North of Domodossola, the Alpine nappe system is cut across by the Centovalli-Simplon lineament.

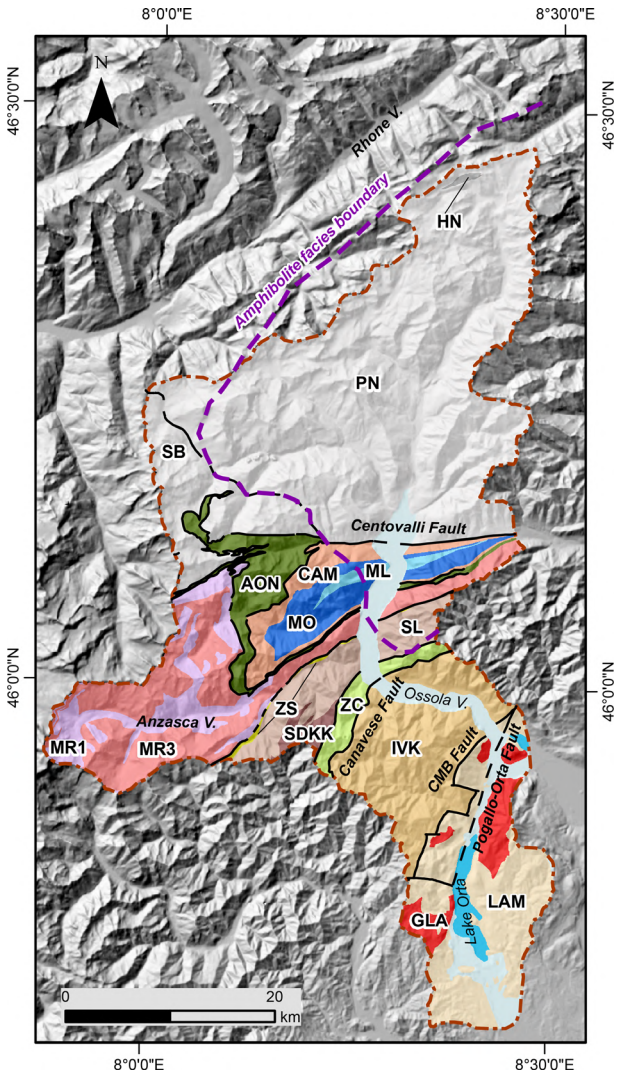

Fig. 2. Geological sketch of the Toce catchment and the Orta Valley summarized after Swisstopo (2005) and Piana *et al.* (2017). Labels of the geological units: AON = Antrona Zone; CAM = Camughera; GLA = Laghi granites; HN = Helvetic Nappes; IVK = Ivrea-Verbano Zone; LAM = Laghi Series; ML = Monte Leone; MO = Moncucco-Orselina; MR = Monte Rosa; PN = lower Penninic nappes; SB = San Bernardo; SDKK = II Zona Diorito-kinzigitica; SL = Sesia Lanzo; ZC = Canavese Zone; ZS = Zermatt-Saas.

The Orta Valley is situated in the western South Alpine domain dominated by Palaeozoic metamorphic rocks called Massicio dei Laghi (MdL), which were intruded by Early Permian plutons (Swisstopo 2005; Piana *et al.* 2017). The MdL is divided into the Ivrea-Verbano Zone (IVK) and the Serie dei Laghi (LAM) separated by the Cossato-Mergozzo-Brissago (CMB) tectonic line (Fig. 2). The CMB line is cross-cut by a younger fault zone, the Pogallo-Orta fault. It is likely that the topographically lower relief of the Orta Valley has been structurally conditioned by the zone of weaker rock corresponding to the Pogallo-Orta fault.

The Lake Orta (Fig. 3A), also called Cusio (18.2 km^2, 12.4 km long and 2.5 km wide), is the westernmost and highest (lake level at 290 m a.s.l.) of the Italian valley lakes fringing the Alps. Lake Orta reaches a maximum depth of 143 m (71 m on average) in the northern sector, while in the shallower southern sector the Island of San Giulio sticks out. The catchment basin (116 km^2) has longer tributary valleys on the western side (Fiumetta, Qualba, Pellino and Plesna tributary valleys), where it reaches its maximum elevation at Mt. Croce (1643 m a.s.l.) on the watershed between the Orta basin and the Sesia Valley (Fig. 1B). On the opposite, eastern side a low mountain ridge separates the Orta basin from the bigger Lake Maggiore (lake level at 196 m a.s.l.) and reaches the Mottarone summit at 1491 m a.s.l. with the Pescone Valley carved in the southern side. The valley sides are very irregular, with several spurs. Small tributary valleys are located to the west, while the eastern side is characterized by flatter morphology of the Armeno-Miasino plateau. This latter is cut by the Agogna River flowing down the southern side of Mottarone.

The Orta Valley is interpreted as having formed primarily during the Mediterranean salinity crisis of the Messinian (Bini *et al.* 1978; Finckh 1978). Subsequent reshaping took place repeatedly during the many glacier advances associated with the Pleistocene cold phases (Felber & Bini 1997; Pfiffner *et al.* 1997).

The Quaternary succession is mostly comprised of glacial deposits forming a small amphitheatre (about 30 km^2) just before the outlet of the valley (Fig. 3). Glacial deposits are also scattered along the valley slopes and partially fill the lower Strona Valley to the northwest and the flat area between Armeno and Miasino. To the southeast the Orta amphitheatre merges with the large Verbano end-moraine system (Bini *et al.* 2014). The glacifluvial deposits south of the lake, which are presently being in part reworked by the Agogna River, merge into the larger Sesia and Ticino glacifluvial fans (Piana *et al.* 2017).

Material and methods

Geomorphological mapping

Several field surveys were carried out during the years 2014 and 2015. In order to find erratic boulders, most of the ridges previously mapped as moraines were visited. Geomorphological and sedimentological characteristics were noted (pebble composition, consolidation degree, weathering degree, Munsell colour, etc.). Further geomorphological analyses were performed through high-resolution (5 m) LIDAR data sets, which are available from the Geoportale of Piemonte (http://www.geoportale.piemonte.it) and were then processed using contour lines and hillshade of ArcGIS (10.4). The obtained digital elevation model (DEM, Fig. 3A)

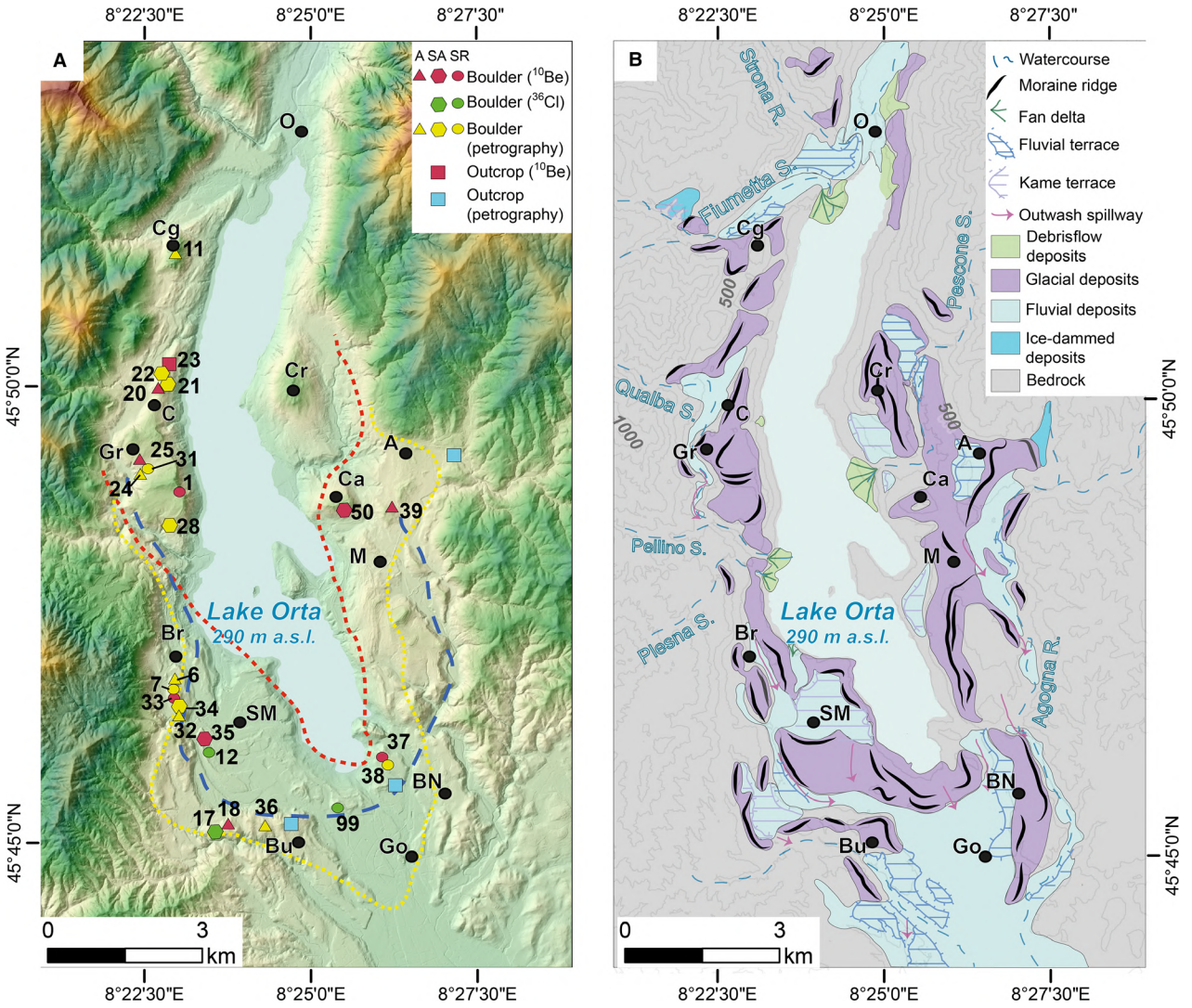

Fig. 3. A. DEM of the Orta Valley (location in Fig. 1) with location of boulders (A = angular, SA = subangular, SR = subrounded) and outcrops. Dashed lines represent interpretations of extent of Orta Glacier during LGM: yellow (Castiglioni 1940); blue (Penck & Brückner 1901–1909), red (Bini *et al.* 2009). B. Geomorphological sketch of the Orta Valley. In both, the localities are marked by black dots and labelled as follows: A = Armeno; BN = Bolzano Novarese; Br = Briallo; Bu = Bugnate; C = Colma; Ca = Carcegna Mt.; Cg = Cregno Mt.; Cr = Crabbia Mt.; Go = Gozzano; Gr = Grassona; M = Miasino; O = Omegna; SM = San Maurizio d'Opaglio.

helped to extend the glacial morphologies recognized in the field and make correlations. A geomorphological map (Fig. 3B) combining field observations and the digital landscape analysis for the Orta area includes sediment and landform distribution over the bedrock.

^{10}Be surface exposure dating

A total of 25 rock samples (Table 2) was collected in the summer of 2014 on lateral and frontal moraines in order to obtain a representative chronology of the several moraine ridges across the whole extent of the amphitheatre. Boulder samples were taken from the highest suitable surface of the largest erratic boulders (Fig. 4). Selection criteria for the eligibility of boulders were their location, stability, size and appearance. All surfaces with evidence of spalling or working by man were avoided. For most of the sampled boulders, long-lasting postdepositional cover can likely be excluded, as most of them are located on the crests of the ridges. As the age of a rock surface is quite easily affected by the postdepositional history of the boulder (human impact, slope processes, weathering, etc.), sampling was done on smooth surfaced boulders with protruding quartz veins, as they represent the untouched appearance of a slowly eroding boulder. Some boulders showed clear glacial striae, which are another indication for little postdepositional erosion. Samples of about 800 g and no thicker than 4 cm were taken with saw, hammer and chisel. Exact location,

Table 1. Overview of the geological units of the Toce catchment.

Unit label	Geological unit	Metamorphic degree	Petrography	References
IVK	Ivrea-Verbano	Pre-Alpine amphibolite to granulite facies	Garnet, biotite, plagioclase, quartz and sillimanite metapelites	Rutter *et al.* (2007), Piana *et al.* (2017)
LAM	Serie dei Laghi	Pre-Alpine amphibolite facies	Garnet, biotite, plagioclase, quartz, sillimanite and muscovite metapelites	Boriani *et al.* (1990)
GLA	Graniti dei Laghi	None	Granite, granodiorite	Pinarelli *et al.* (1993)
ZC	Canavese Zone	Alpine greenschist facies	Gneiss, schists, Permian diorite, serpentinites, and sedimentary carbonate and siliceous rocks	Ferrando *et al.* (2004)
SL	Sesia-Lanzo Zone	Pre-Alpine amphibolite facies overprinted by Alpine eclogite facies	Albite, white mica orthogneisses and schists; jadeite pyroxene, garnet micaschists; omphacite pyroxene, glaucophane ± chloritoid eclogites and glaucophanites	Compagnoni *et al.* (1977)
SDKK	II Zona diorito-kinzigitica	Pre-Alpine amphibolite facies overprinted by Alpine amphibolite/greenschist facies	Sillimanite, garnet and biotite gneisses; chloritoid, garnet micaschists	Reinhardt (1966)
ZS	Zermat-Saas	Alpine eclogite facies	Omphacite pyroxene, glaucophane ± chloritoid eclogites and glaucophanites; serpentinites	Ernst & Dal Piaz (1978)
MR	Monte Rosa	Alpine eclogite facies	K-feldspar megacrysts metagranitoids (MR3); albite, quartz, white mica, chlorite and garnet fine-grained gneiss (MR1); chloritoid, phengite, garnet ± kyanite, talc, chlorite micaschists (MR1)	Frey *et al.* (1974), Keller *et al.* (2005)
SB	San Bernardo	Alpine amphibolite facies	Paragneiss, micaschist, orthogneiss and amphibolite	Bigioggero *et al.* (1981), Piana *et al.* (2017)
AON	Antrona Zone	Alpine eclogite to amphibolite facies	Garnet, glaucophane and omphacite clinopyroxene metabasites; serpentinites	Colombi & Pfeifer (1986), Turco & Tartarotti (2006)
MO	Moncucco-Orselina Zone	Alpine eclogite to amphibolite facies	Biotite, white mica, garnet and staurolite paragneiss; graphitic schists; basic metavolcanites	Bigioggero *et al.* (1981)
CAM	Camughera Zone	Alpine eclogite to amphibolite facies	Biotite, white mica, garnet and staurolite micaschists and metagranitoids	Keller *et al.* (2005)
PN	Lower Penninic nappes (Monte Leone, Lebendun, Verampio and Antigorio)	Alpine amphibolite to greenschists facies	Garnet, biotite, white mica, staurolite and sillimanite melapelites; hornblende and garnet metabasites	Bigioggero *et al.* (1981), Berger *et al.* (2012)
HN	Helvetic nappes	Alpine greenschists	Biotite, white mica, ± garnet micaschists	Oberhänsli *et al.* (2004)

elevation, thickness of the sample, topographic shielding, dip direction, and dip were noted for the final age calculation.

All 25 collected samples were crushed and underwent quartz separation procedures. Of these, 13 were finally processed, 10 for ^{10}Be and three for ^{36}Cl. All chemical extraction was done in the cosmogenic nuclide surface exposure dating lab at the department of Ion Beam Physics at ETH Zurich. Details of sample preparation at ETH, and a complete and detailed description of surface exposure dating with cosmogenic nuclides, are given in Ivy-Ochs & Kober (2008). Preparation of the beryllium samples follows the method of Kohl & Nishiizumi (1992) as modified by Ivy-Ochs (1996). After crushing the samples to grain size smaller than 1 mm, the samples were leached with HCl and dilute HF (4%) to obtain a pure quartz mineral separate. ^{9}Be carrier was added to the obtained quartz, before dissolving in concentrated HF. Beryllium was isolated with ion exchange columns and pH-selective precipitations. ^{10}Be/^{9}Be ratios were measured with accelerator mass spectrometry (AMS) using the 600 kV TANDY system (Christl *et al.* 2013) at the Laboratory of Ion Beam Physics at ETH Zürich against the in-house standard S2007N (Christl *et al.* 2013), which is calibrated to 07KNSTD (Nishiizumi *et al.* 2007). Measured ratios were corrected with the full-process blank of $(3.6\pm2.6)\times10^{-15}$.

Table 2. Location and provenance of the studied boulders.

Sample number	Locality	Coordinates		Petrography	Unit	Roundness
		Lat. °N	Long. °E			
1	Antenna	45.814	8.381	Granite	GLA	SR
6	Briallo	45.777	8.379	Fine-grained gneiss	MR3	A
7	Briallo	45.775	8.381	Metagranite	MR3	SR
11	Puffer	45.858	8.379	Gneiss	IVK	A
12	Curlera	45.769	8.381	Garnet micaschist	SL	SR
17	Bugnate	45.753	8.394	Garnet amphibolite	AON	SA
18	Bugnate	45.754	8.395	Fine-grained gneiss	MR3	A
20	Colma	45.835	8.376	Garnet micaschist	SL	A
21	Colma	45.836	8.377	Garnet micaschist	SL	SA
22	Colma	45.839	8.379	Garnet micaschist	SL	SA
23a	Colma	45.840	8.379	Gneiss	LAM	Bedrock
24	Grassona	45.816	8.371	Kinzigite	IVK	A
25	Grassona	45.818	8.370	Micaschist	SL	A
28	Egro	45.816	8.378	Gneiss	IVK	SA
31	Grassona	45.816	8.371	Garnet micaschist	SL	SR
32	Briallo	45.775	8.380	Amphibolite	AON	A
33	Briallo	45.778	8.379	Granite	GLA	SA
34	Briallo	45.777	8.379	Orthogneiss	MR3	SA
35	Curlera	45.769	8.387	Fine-grained gneiss	MR3	SR
36	Bugnate	45.754	8.401	Fine-grained garnet gneiss	SL	A
37	Buccone	45.766	8.434	Quartzite	ZC	SR
38	Buccone	45.765	8.434	Garnet micaschist	CAM	SR
39	Armeno	45.813	8.436	Garnet micaschist	CAM	A
50	Carcegna	45.812	8.423	Granite	GLA	SA
99	Hitsch	45.757	8.421	Fine-grained gneiss	MR3	SR

We calculated exposure ages with the CRONUS-Earth online calculator (Balco *et al.* 2008), applying the northeast North America (NENA) production rate of 3.87 ± 0.19 at g^{-1} a^{-1} (Balco *et al.* 2009) and the scaling scheme of Lal (1991) and Stone (2000). The NENA production rate is in excellent agreement with the ^{10}Be production rate recently determined in the Alps (Claude *et al.* 2014), as well as those published by Borchers *et al.* (2016). No snow cover correction has been applied. We are aware that postdepositional climate allowed for snow cover on elevations as low as the research area, but any assumed snow cover could be as wrong as setting it to zero for all samples. An erosion rate of 1 mm ka^{-1} (André 2002) was used for both the bedrock and the erratic boulders. The errors listed in Table 3 are the internal error (1σ) (which includes the AMS standard reproducibility, counting statistics, standard mean error of samples and uncertainty of the blank correction).

^{36}Cl surface exposure dating

Chlorine was extracted from samples Curlera 12, Bugnate 17 and Hitsch 99 (grain size 88–500 μm). Poor quartz yield from these samples led to the use of ^{36}Cl. The whole-rock extraction procedure follows the methods of Stone *et al.* (1996) and Ivy-Ochs (1996) using isotope dilution with a ^{35}Cl-enriched spike (Ivy-Ochs *et al.* 2004b; Desilets *et al.* 2006). Approximately 30 g of whole rock was dissolved with concentrated HF and HNO_3. Cl was precipitated with addition of Ag. ^{36}S (interfering isobar) was removed through precipitation of $BaSO_4$. ^{36}Cl AMS measurements were done at the LIP 6 MV TANDEM system at ETH Zurich relative to the internal K382/4N standard (Synal *et al.* 1997; Christl *et al.* 2013; Vockenhuber *et al.* 2019). Uncertainties on reported concentrations (1σ) include AMS standard reproducibility, counting statistics, and the standard mean error of the samples. Major and trace element concentrations (as required for age calculation) were determined on aliquots of each leached sample with ICP-MS at Act labs S.A. (Ontario, Canada) (Table S1).

^{36}Cl exposure ages were calculated with the in-house MATLAB code implementing the equations and constants given in Alfimov & Ivy-Ochs (2009). The following sea level, high latitude spallation production rates were used: 48.8 ± 3.4 at g_{Ca}^{-1} a^{-1} (Stone *et al.* 1998), 162 ± 24 at g_{K}^{-1} a^{-1} (Evans *et al.* 1997), 13 ± 3 at g_{Ti}^{-1} a^{-1} (Fink *et al.* 2000) and 1.9 ± 0.2 at g_{Fe}^{-1} a^{-1} (Stone *et al.* 2005) with scaling after Stone (2000). Production of ^{36}Cl at the rock surfaces due to muon interactions amounts to 9% from Ca (Stone *et al.* 1996, 1998) and 6% from K (Evans *et al.* 1997). Calculation of ^{36}Cl produced through (epi-) thermal neutron capture on ^{35}Cl follows the methodology of Alfimov & Ivy-Ochs (2009 and references therein) using a neutron flux value of 760 n g_{air}^{-1} a^{-1}. The applied constants and production rates are well in agreement with values recently reported by Borchers *et al.* (2016) and Marrero *et al.* (2016).

Fig. 4. Photographs of sampled boulders (red arrow shows the sampling spot) and outcrops. A. Bugnate 17. B. Grassona 25. C. Bugnate 18. D. Briallo 33. E. Carcegna 50. F. Colma 20. G. Armeno 39. H. Outcrop of stratified gravel and sand deposits east of Armeno related to damming of the Agogna River by the Orta Glacier during the maximum stand.

Table 3. Sample information, AMS data and calculated exposure ages for boulders dated with cosmogenic ^{10}Be or ^{36}Cl.

Sample	Lat. °N	Long. °E	Elevation (m a.s.l.)	Thickness (cm)	Shielding factor	^{10}Be 10^4 atoms g^{-1}	Exposure age ka[3]
Colma 20	45.835	8.376	556	2	0.977	11.085±0.797	18.01±1.32 (1590)
Colma 23a[1]	45.840	8.379	493	1.5	0.817	6.580±0.425	13.28±0.87 (1080)
Grassona 25	45.818	8.370	519	1.5	0.959	10.991±0.629	18.71±1.09 (1430)
Antenna 1	45.814	8.381	596	3	0.993	5.387±0.468	8.310±0.73 (830)
Briallo 33	45.778	8.379	517	1.5	0.981	14.445±1.586	24.25±2.73 (2980)
Curlera 35	45.769	8.387	442	3	0.981	6.629±0.695	11.86±1.26 (1390)
Bugnate 18	45.754	8.395	520	2	0.923	12.712±0.728	22.63±1.33 (1730)
Buccone 37	45.766	8.434	417	3	0.992	12.506±0.700	22.88±1.31 (1730)
Armeno 39	45.813	8.436	504	1.5	0.930	10.798±0.589	19.19±1.07 (1420)
Carcegna 50	45.812	8.423	595	2	0.990	17.810±1.224	27.94±1.98 (2410)
						^{36}Cl	
Bugnate 17[2]	45.753	8.394	522	3	0.973	12.939±1.220	20.45±1.93 (2040)
Curlera 12[2]	45.769	8.381	445	2	0.918	32.877±3.510	19.38±2.07 (2750)
Hitsch 99[2]	45.757	8.421	399	2	0.980	19.890±2.390	19.30±2.32 (2400)

[1]Bedrock.
[2] ^{36}Cl dating.
[3]External uncertainty in the bracket.

Glacier reconstruction

Based on the results of this work, a new outline for the maximum extent of the Orta Glacier during the LGM is presented. Since our surveys are limited to the Orta lobe of the much larger Toce catchment, the interpretation of Bini *et al.* (2009) was used for depicting the catchment upstream from Gravellona Toce. Previous maps (Jäckli 1970; Ehlers & Gibbard 2004; Bini *et al.* 2009) show the ice extent in the accumulation areas at what was assumed to be their maximal extent during the LGM. However, focusing on the Toce catchment, it appears that the nunataks were drawn either too small or too big. Accordingly, we have slightly modified the outline of the ice extent in the upper Toce catchment for figures in our study. We assumed an equilibrium line altitude (ELA) of around 1500 m a.s.l., which is concordant with the one reported for the Aosta region in the Italian Alps by Forno *et al.* (2010) calculated using the AAR method. Regional ELA values indicated by Florineth & Schlüchter (1998) and Kuhlemann *et al.* (2008) are slightly lower. Considering the high elevation of the accumulation areas of the Toce catchment, slight differences in ELA are irrelevant also considering that ELA is a mean value in a long-lasting period like the LGM.

Flow line reconstruction

Samples of 24 large erratic boulders (>1 m^3) on top of the moraines were collected for thin section petrographic analysis (Table 2) in order to evaluate their provenance and reconstruct glacier flowlines. Many of the lithologies can only come from specific and restricted source outcrops in the upstream catchment. These index erratics can be used to track ice-flow pathways (e.g. Coutterand *et al.* 2009; Jouvet *et al.* 2017), a methodology which has been employed in the Alps for nearly 200 years (Guyot 1847). To assess the relative contribution from the North Alpine and South Alpine domains to the Toce Glacier material, we defined the provenance of the boulders through petrographic characteristics, thus their metamorphic affinity with one or more than one Penninic nappe or with a South Alpine unit (Tables 1, 2). A second approach is based on characteristic boulder roundness that can yield information on transport position in the glacier and transport distance. High angularity is mostly related to passive supraglacial transport, while subangular to subrounded boulders were likely shaped during the transport in sub- or englacial position (Benn & Ballantyne 2005; Benn & Evans 2014) with significant differences due to clast lithology (Lukas *et al.* 2013). However, these works are mostly related to gravel-size clasts, while boulders can have been affected by different shaping and clustering processes (Boulton 1978). The abundance of a particular lithology is also an expression of the distance of the source outcrop from the marginal position (Larson & Mooers 2004). By identifying bedrock source regions (Fig. 2), we could reconstruct flowlines for the Orta glacier. It should be remembered that debris transport histories might involve several glacial cycles during which the ice divides and ice-flow vectors could have shifted dramatically (Benn & Evans 2014). In order to assess the reliability of these data and identify key lithologies from the Toce catchment, we checked the petrography of pebbles within subglacial sediments (Menzies 2003) from marginal positions in three different locations (Fig. 3A) through hand lens and thin-section identifications.

Results and interpretation

Geomorphology of the Orta end-moraine system

The Orta Valley has a rough N–S orientation and the end-moraine system extends at the southern end with a maximum width of about 5 km. The thickness of the

glacial units is normally some tens of metres on the crystalline bedrock, which crops out also in the frontal sector of Gozzano (Fig. 3B). The moraines of the Orta system can mostly be classified as dump moraines. Dumping of englacial and supraglacial debris during prolonged periods of glacier stability leads to the build-up of these ridges of sediment (Benn & Evans 2014). The oscillation of the glacier margin, especially close to the valley sides, can lead to formation of closely spaced lateral moraines and intervening troughs (Benn *et al.* 2003), which are clearly visible in the Orta system. Their preservation is good in flat areas like in the western side or in the Armeno-Miasino plateau (Fig. 3B), where paraglacial activity during deglaciation was weaker than in sectors with steep slopes. The observed glacial sediments span the whole range of grain sizes, from clay (scanty) to house-sized boulders with prevalence of silty sands.

Ridges of the Orta amphitheatre can be subdivided into three belts (Fig. 3B). The outermost glacier position is represented by frontal moraines in the Bugnate-Briallo sector, which are roughly continuous in the western side (Fig. 5), while the moraines located on the southeastern margin are more discontinuous. Lateral moraines on the western side show articulate geometries due to the irregular bedrock morphology with several spurs. Some of the lateral moraines show small arcuate extensions into wind gaps, as for example at Grassona (Fig. 3B). On the eastern valley slope, the presence of the Armeno-Miasino plateau, which is characterized by a relatively flat morphology, and the reshaping of the landscape by the Agogna River led to poor moraine preservation and more discontinuous landforms. The elevation of these external ridges spans from 545 m a.s.l. at Bugnate to 478 m a.s.l. at Bolzano Novarese in the frontal sector. The equivalent lateral moraines have almost the same elevation (Fig. 5) along the left-lateral side at Armeno (525 m a.s.l.) and right-lateral side at Briallo (523 m a.s.l.), with slightly higher elevation upstream at Grassona (612 m a.s.l.). Along these external moraines the samples Bugnate 17 (Fig. 4A), Bugnate 18 (Fig. 4C) and Briallo 33 (Fig. 4D) were dated. The northernmost lateral ridge upstream of Omegna is at 760 m a.s.l. On the opposite eastern side the dated boulder Carcegna 50 (Fig. 4E) is located on the Monte di Carcegna bedrock knob (611 m a.s.l.), which was likely a small nunatak during the LGM.

An internal set of moraines, located 1 to 2 km inwards from the outer belt, shows a maximum elevation of 420 m a.s.l., with the best preserved moraines at Grassona and in the area from Briallo to Bolzano Novarese (Fig. 3). This belt consists of multiple, closely spaced ridges, which suggests an oscillating nature of the Orta Glacier lobe. None of the moraine belts shows continuity over the whole width of the amphitheatre, because they all are strongly incised by coeval and/or subsequent meltwater flow. In this belt several samples (Table 2) were processed for dating: Colma 20 (Fig. 4F), Grassona 25 (Fig. 4B), Curlera 35, Curlera 12, Hitsch 99, Armeno 39 and Buccione 37. In the Orta basin some bedrock hills host scattered boulders, located below the top of the hills, which were in any case interpreted as nunataks. The Carcegna Hill, to the east, and the Egro and Puffer hills, to the west, reach elevations close to the inferred ice surface of previous authors (Castiglioni 1940; Bini *et al.* 2009). Here, the samples Carcegna 50 and Antenna 1 were dated.

A third, discontinuous inner moraine belt, which is located only 150–500 m inwards from the second belt, encircles the lake shore. The S. Maurizio d′Opaglio village is built on a flat area at 360–370 m a.s.l. that likely formed as wide marginalproglacial outwash fan between the two moraine belts. Only the bedrock sample (Colma 23) can be referred to the margin of the glacier during this stadial in our reconstruction (Fig. 6).

Surface exposure dating

^{10}Be and ^{36}Cl exposure ages range from 8.3±0.7 to 27.9±2.0 ka (Table 3). Three samples show dates much younger than their positions would suggest (Fig. 5); these are Antenna 1 (8.3±0.7 ka), Colma 23a (13.3±0.9 ka) and Curlera 35 (11.9±1.3 ka). LGM glaciers in the Alps had retreated back into higher mountain valleys long before 13.3 ka, the age of Colma 23a (Pellegrini *et al.* 2005; Ravazzi *et al.* 2014; Ivy-Ochs 2015; Federici *et al.* 2017). Explanation for these clearly too young ages is to be found in weathering (Antenna 1) or burial by sediment (bedrock Colma 23a and possibly Antenna 1). Postdepositional toppling of boulders Antenna 1 and Curlera 35 cannot be ruled out. Colma 23a was sampled on bedrock protruding not more than 40 cm above the soil at present, and it therefore was likely buried by glacial sediment for a significant amount of time. The well-preserved glacial striations verify that the glacier definitely did override this location, but the resulting age indicates that the surface had been buried and protected.

From the remaining samples, we recognize two clusters that exist both in the overlapping ages and in their geographical position (Fig. 5). The older cluster consists of Bugnate 18 (22.6±1.3 ka), Briallo 33 (24.3±2.7 ka) and Carcegna 50 (27.9±2.0 ka). The two older ages correlate to the furthest extent of moraines that we found boulders on, thereby representing the maximum extent of the LGM. The Bugnate 17 ^{36}Cl age (20.5±1.9 ka) belongs to the same geomorphological context.

The younger cluster consists of the Colma 20 (18.0±1.3 ka), Grassona 25 (18.7±1.1 ka), Buccone 37 (22.9±1.3 ka) and Armeno 39 (19.2±1.1 ka) ^{10}Be dates. In addition, ^{36}Cl dates for Curlera 12 (19.4±2.1 ka) and Hitsch 99 (19.3±2.3 ka) have been determined. The ages of this unit are consistent with a smaller glacier extent, traceable over the whole width of the amphitheatre, with its frontal moraines situated 1 to 2 km inwards from the older more external moraines. The age of sample

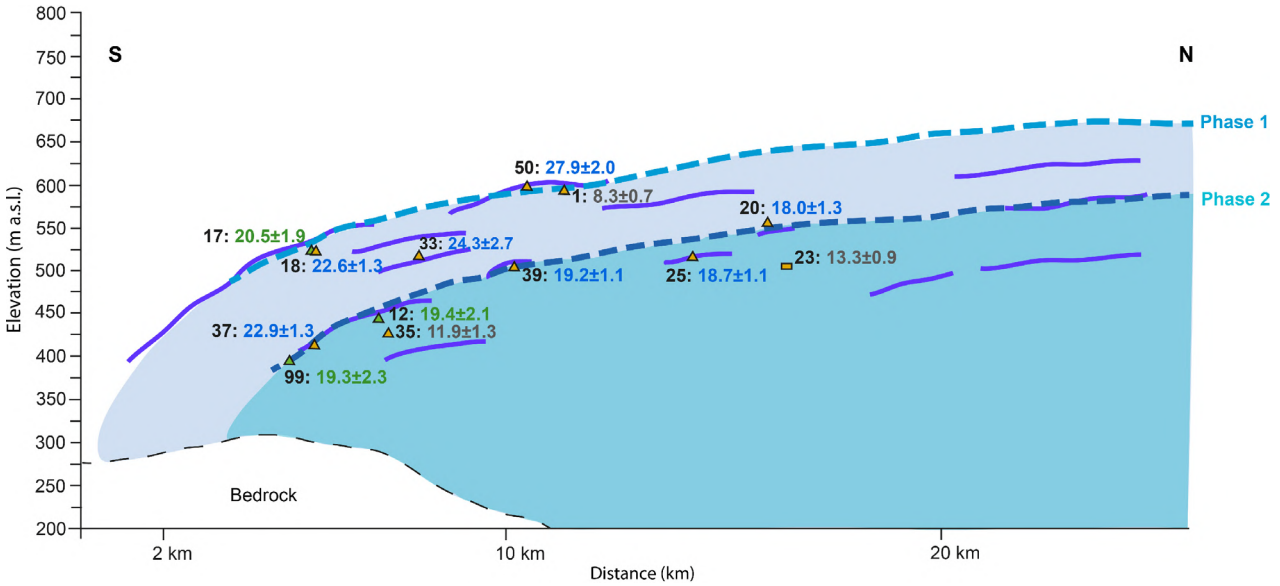

Fig. 5. Longitudinal sketch of the Orta end-moraine system. Moraine ridges (both western and eastern sides) are represented by thick violet lines, dated boulders locations are plotted as triangles, the rectangle represents the dated bedrock surface (yellow for the ^{10}Be and green for ^{36}Cl datings), black label is the boulder number (Tables 2, 3) and ages are represented in ka (^{10}Be in blue; ^{36}Cl in green and outliers in grey). Dashed lines show the two main moraine belts for which dates have been determined. A lower and inner set of ridges likely represents the start of ice-decay.

Buccone 37 (22.9±1.3 ka) fits with the ages of the onset of glacier retreat from the outer moraines. However, its position in the landscape does not fit with the outline of this glacial stage. The bedrock knob where the sampled boulder was deposited might have been protruding from the ice soon after the glacier began to retreat from its maximum extent, making deposition of erratic boulders possible before the ice retreated north of this point. We therefore regard this age as belonging to the maximum extent of the LGM.

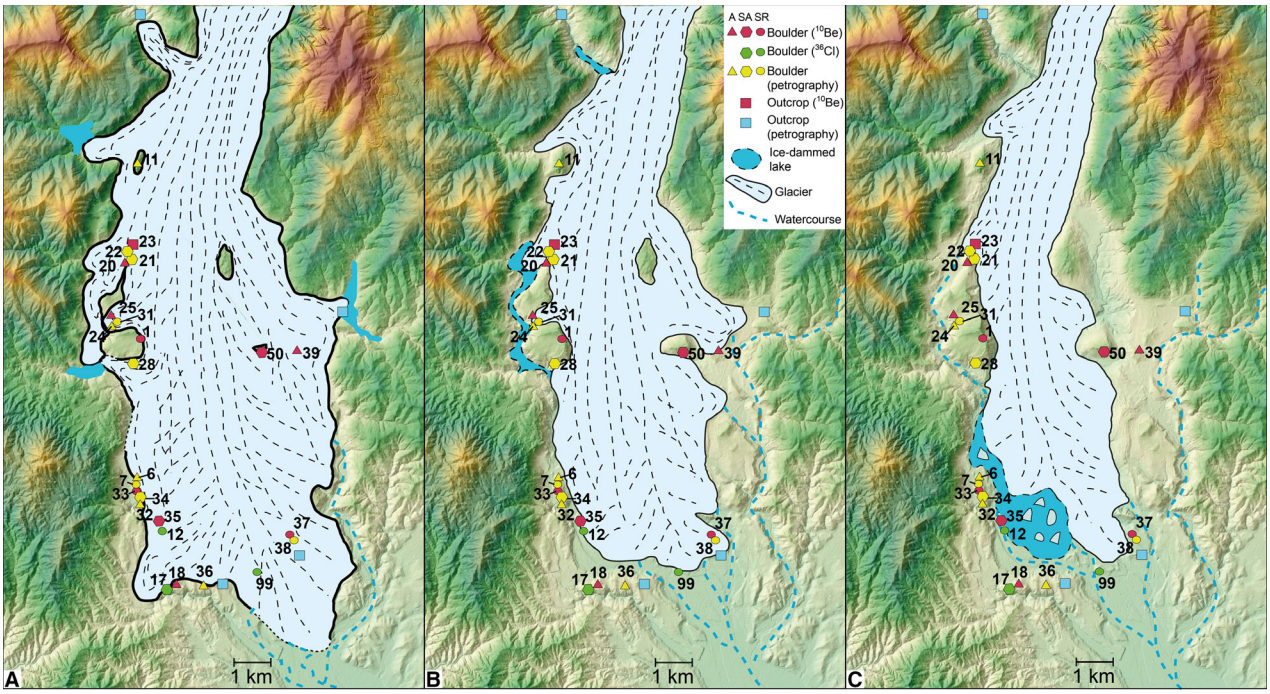

Fig. 6. A–C. Reconstruction of the Orta Glacier lobe during the three main phases recognized in the amphitheatre. The numbers refer to the boulders as in Table 2, the legend of the boulders refers to Fig. 3.

Glacier reconstruction

The reconstruction of two major glacial stages of the Orta glacier (Figs 5, 6) relies on the combination of surface exposure dating and geomorphological analysis. We assumed symmetrical heights for the two sides of the glacier and a surface slope of the Orta lobe similar to the one mapped by Bini *et al.* (2009), which is around 4.5% (600 m vertical drop over 13.5 km length at the glacier centre line).

The inferred ELA of about 1500 m a.s.l. allows the presence of small local glaciers originating from the higher regions of the Strona valley (Fig. 7). It is assumed that these glaciers did in any case not merge with the Orta glacier because of the length and the shape of the Strona Valley. Figure 6A presents the furthermost extent of the Orta glacier during the LGM, which is an average because spatial and temporal variations existed due to factors like sub-millennial fluctuations, bed topography and debris cover.

On the southern slope of the Bugnate ridge, the marked weathering of the bedrock supports the hypothesis that ice did not reach any further south during the LGM. On the right-lateral side, the maximum extent was mostly restricted due to bedrock topography. Minor glacier tongues of the Orta lobe made it into the Strona and Fiumetta Valleys (Fig. 6A). However, they did not cover, for example, the strongly consolidated basal till located in the Strona Valley (Fig. 6A). This contains a variety of clasts, amongst which lithologies of the Penninic basement that suggests a provenance from the Anza-Toce catchment. The colour of the matrix (7.5YR Munsell) and the extensive weathering of the clasts point to a pre-LGM age. Therefore, in our glacier reconstruction this location is regarded as having been ice-free during the LGM and contradicts the ideas postulated by Penck & Brückner (1901–1909) and Hantke (1983) that significant ice filled the Strona Valley during the last glaciation.

The glacier tongue overriding the Armeno plateau could have dammed the Agogna River during the LGM maximum extent, leading to formation of marginal lakes (Fig. 6A). The Agogna River was fed by meltwater of the Verbano branch of the Ticino glacier (Fig. 7). We interpret the more than 20-m-thick deposit east of Armeno, along the Agogna Valley, as representing continuous sedimentation in an ice-marginal alluvial/deltaic environment. The outcrop is made up of centimetric to decametric coarsening upward graded beds of silt and sands (Fig. 4H) interbedded with fine to coarse gravels. The ice-dammed lake was fed by both glacier meltwater and the Agogna and Ondella rivers (Fig. 6A).

Just south of the Fiumetta Valley, the glacier outline is based on the rich spectrum of erratic boulders. The summit of Cregno Mt. (Fig. 3, 683 m a.s.l.) has been interpreted as ice-free, based on the line of erratic boulders found around 15 m below the top. Similar to Cregno Mt., on the opposite side of the lake a line of erratics was found just below the top of Carcegna Mt. (Fig. 3, 611 m a.s.l.), pointing to an ice-free summit of the hill made up of metamorphic bedrock.

A younger glacial phase, related to an age between 19–18 ka, is outlined in Fig. 6B. The related moraine belt around the southern tip of the present-day lake expresses the oscillating nature of the glacier during that interval. The glacier retreated up to 2 km from its maximum extent. On the right-lateral side, the ice withdrew almost completely from the Strona and Fiumetta Valleys and the hilltops around Grassona were largely ice-free. Rivers were undammed on the left lateral side and meltwater on all sides of the glacier started reworking the moraines and sediment cover of the previous extent. On the eastern side, Crabbia Mt. (Fig. 3, 662 m a.s.l.) can be assumed to be ice-free, inferred from the glacier's surface elevation. No sediments or boulders have been found on this hilltop, although the numerous ruins found on top were likely built out of erratic blocks left behind here by the retreating glacier.

The downwasting of the Orta Glacier at about 18 ka (Fig. 6C) led to the formation of large ice-marginal lakes connected to the outwash plain. Meltwater flowing southwards cut the lower moraines closely surrounding the southern lake tip, whilst the Agogna River continued flowing in its current channel. During glacier withdrawal, but before drainage switched northwards, meltwater found its way through and in between existing moraines, leading to breaching of both the inner and outer frontal moraine belts. Slope parallel channel morphologies and moraine entrenchments are presently windgaps. During this latest stable phase in the Orta Valley, a proglacial lake formed in the overdeepened basin, draining southwards until the glacier retreated as far north as Gravellona Toce. From that moment, the Lake Orta outlet drained northwards and evolved to its present-day setting.

Flowline reconstruction

The provenance of 24 boulders (12 dated and 12 undated) has been assessed (Table 2). Specific assignment is possible in part due to the particular geological setting of the Toce catchment, characterized by the juxtaposition of several tectonic slices of different metamorphic degree (Table 1, Fig. 2). Four samples (Antenna 1, Colma 23, Briallo 33, Carcegna 50) are granites (GLA) and mica schists (LAM) of the bedrock surrounding Lake Orta. The other boulders show the petrographic signature of the Ivrea-Verbano crystalline basement (IVK: Puffer 11, Grassona 24), of the Sesia-Lanzo Zone (SL: Curlera 12, Colma 20, 21, 22, Grassona 25, 31, Egro 28, Bugnate 36) and of the metagranitoids of the Monte Rosa massif (MR3: Briallo 6, 7, 34, Curlera 35, Bugnate 18, Hitsch 99), while two are attributable to the Antrona Zone (AON: Bugnate 17 and Briallo 32), two to the

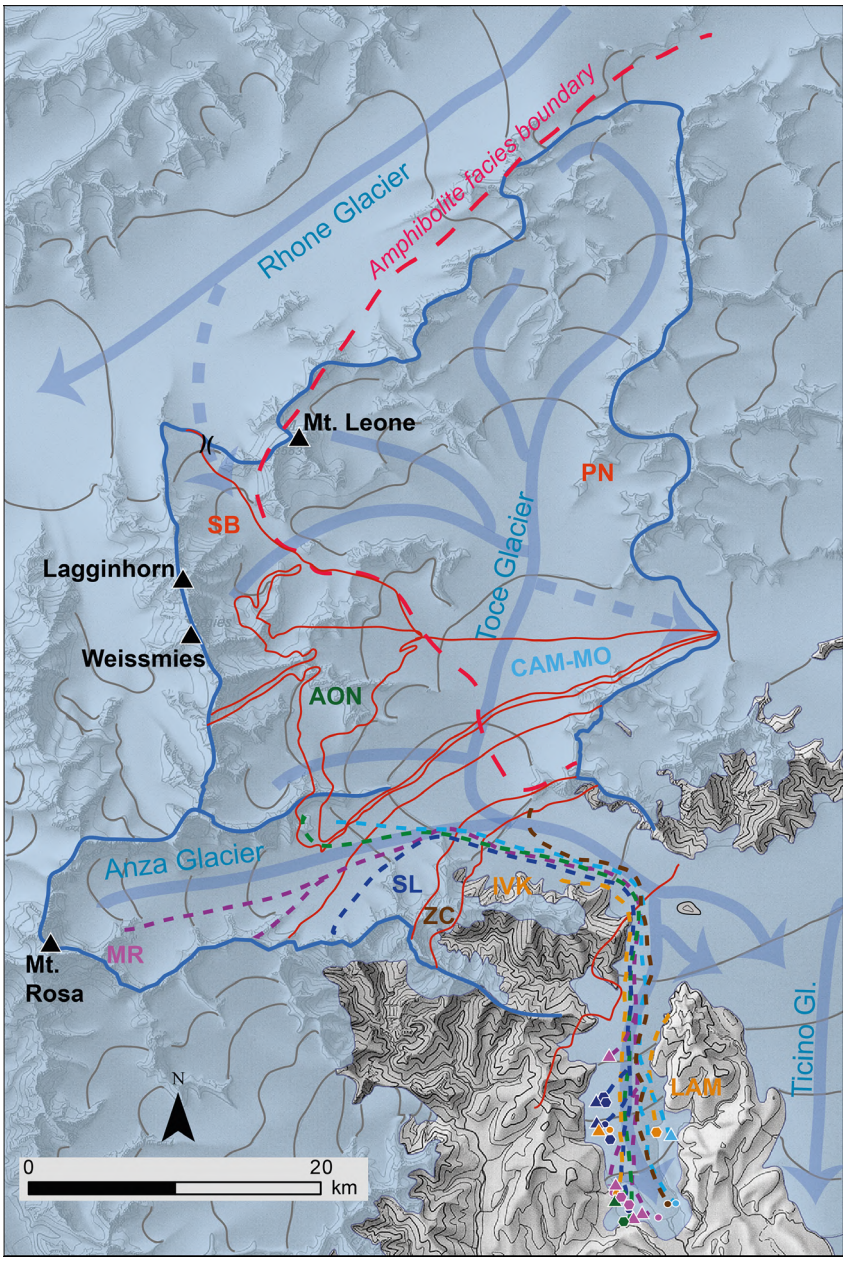

Fig. 7. Reconstruction of the ice-flow paths (pale blue arrows after Bini *et al.* 2009) and the transport paths of the studied boulders from the source area (dashed lines), map as in Fig. 1B. Geological units are labelled as in Fig. 2 and Table 1, boulder symbols are as in Fig. 3; colours of the boulders and paths are the same as the label of the provenance unit.

Camughera nappe (CAM: Buccone 38, Armeno 39) and one to the Canavese Zone (ZC: Buccone 37). It is remarkable that all of them belonged to the Anzasca Valley or to the lower Ossola Valley, downstream of the junction with the Anzasca Valley. The same result came from glacial deposits in three locations of the amphitheatre (Fig. 3A) where clasts were collected, some of them for thin sections. No boulders show a provenance related to the upper Ossola Valley or the northern tributaries. Notably, no boulders coming from possible transfluence from the Rhone glacier through the Simplon Pass (Kelly *et al.* 2004) were recognized.

The boulders are mostly characterized by hard and anisotropic lithologies, so lithological bias weakly affected their degree of roundness (Lukas *et al.* 2013). Most of the angular and subangular boulders belong to the outer moraines of the western sector of the amphitheatre (Figs 3A, 7). By contrast, the subrounded ones are related to the lower and more internal moraines (Figs 3A, 7). This suggests en-/subglacial transportation

and subsequent deposition during the oscillation of the glacier front after the maximum stand.

The results allow us to infer the relationship between the source outcrop areas and, as a consequence, the path they made through the ice conveyor belt (Fig. 7). The western sector of the Orta amphitheatre shows provenance from the Anzasca Valley while the frontal sector and the eastern side have boulders possibly coming also from the lower Ossola Valley. The lack of observed lithologies from the inner Toce catchment (lower Penninic nappes) can also be ascribed to the longer pathways to cover, but also from the abundance of weak rocks (metapelites) in these geological units that are more sensitive to breaking apart during transport.

Discussion

Waxing and waning of the Orta Glacier

The reconstruction and chronology of the Orta end-moraine system show three major moraine belts pointing to a glacier snout standing close to the maximum position. The older stage, as outlined by the Bugnate and Briallo moraines and the Carcegna hill, is interpreted as the maximum extent of the Orta Glacier during the LGM. This culmination took place between 26.5–23 ka; this is in agreement with the chronology available from other end-moraine systems in the Alps (Monegato *et al.* 2007, 2017; Ivy-Ochs *et al.* 2018) that point to a maximum extent during Greenland Stadial 3 (Fig. 8). Three ages (Bugnate 17 and 18, Briallo 33) point to a maximum stand of the glacier snout at 24–23 ka, but, considering the standard deviation and the Carcegna 50 age (27.9±2.0 ka), the age could be slightly older. We conclude that the newly interpreted Orta Glacier tongue was less extensive into the Strona and Fiumetta Valleys (Penck & Brückner 1901–1909) but extended much farther south than the extent of Bini *et al.* (2009) (Fig. 3A).

A subsequent retreat of the Orta Glacier was followed by an inferred stabilization or re-advance between 19–18 ka, as assessed by six ages from the second moraine belt (Fig. 5). A third small belt located just in the inner position did not provide suitable boulders to date (Fig. 6C), but it should be slightly younger, just before the final collapse of the Alpine glaciers at 18–17.5 ka (Ravazzi *et al.* 2014; Rossato & Mozzi 2016; Wirsig *et al.* 2016). Such an occurrence of multiple phases during the end of the LGM has been widely reported for many end-moraine systems throughout the Alps (e.g. Ivy-Ochs *et al.* 2004a; Monegato *et al.* 2007, 2017; Ravazzi *et al.* 2014; Reber *et al.* 2014; Salcher *et al.* 2015). Constraining the time gap between subsequent advances has however proven to be difficult and, moreover, this length seems to vary between Alpine regions.

As transfluence occurred from the upper Rhône Glacier into the Toce catchment (Florineth & Schlüchter 1998), it is interesting to consider this glacier's LGM activity phases. Mandier *et al.* (2003) distinguish two stadials between 30 and 18 ka BP, which could be consistent with the two stages presented in this study. Ivy-Ochs *et al.* (2004a) conducted surface exposure dating on Rhône Glacier's moraines and found that the glacier withdrawal from the outermost position started no later than 24±2 ka (recalculation in Ivy-Ochs 2015). Directly descending from the Rhône ice dome and the upper parts of its transecting Rhône Glacier is the ice that flows into the Toce catchment over the present-day Simplon Pass

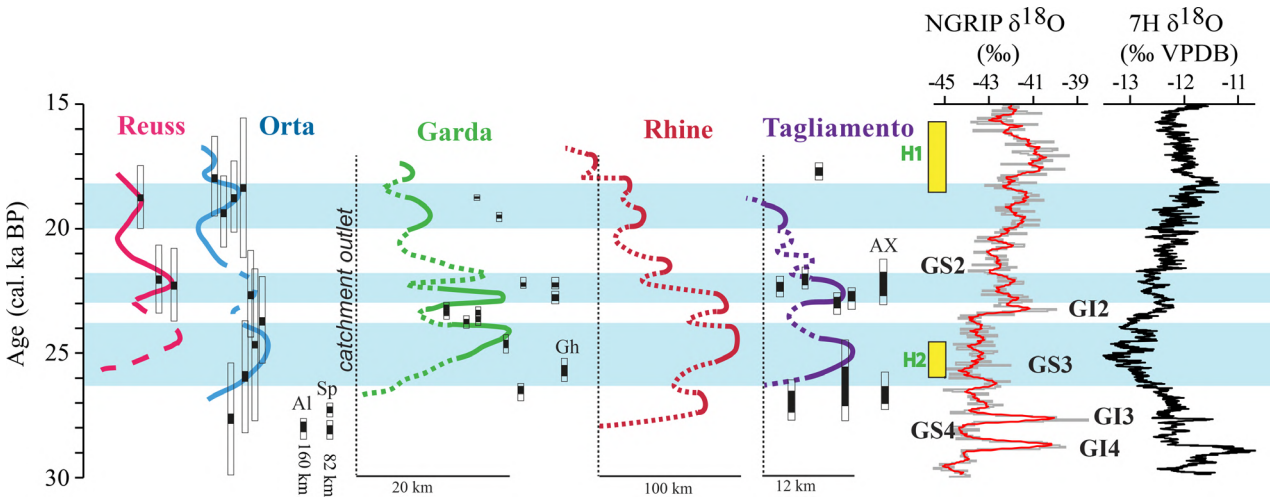

Fig. 8. Major culminations of Alpine glaciers (blue banners) during the LGM from selected end-moraine systems compared to the Orta chronology (Reuss after Reber *et al.* 2014; Orta: this work; Garda after Monegato *et al.* 2017; Rhine after Preusser *et al.* 2011; Tagliamento after Monegato *et al.* 2007), compared with Heinrich Events (Naughton *et al.* 2009), the NGRIP $\delta^{18}O$ record (Svensson *et al.* 2006) and the 7H $\delta^{18}O$ record from speleothems at Sieben Hengste (Luetscher *et al.* 2015). Dates are reported with error bars (Al = Albeins; AX = Azzano Decimo; Gh = Ghedi; Sp = Spormaggiore).

(Fig. 7). For this mountain pass, Dielforder & Hetzel (2014) reported ice-surface lowering at 18±1 ka. Although the chronology of the Orta Glacier is in a general sense in good agreement with these studies, the sensitivity of the Toce catchment towards the input of the Rhône ice dome is not sufficiently understood (Jouvet *et al.* 2017).

The merging of the Toce Glacier with the larger Ticino Glacier likely occurred east of Gravellona Toce (Fig. 7). Despite conflicting interpretations of palaeoglacier reconstruction by previous authors (Castiglioni 1940; Bini *et al.* 2009), according to the petrography of the boulders collected in the eastern side of Orta Valley (Buccone 37 and 38, Armeno 39) a provenance from the Ticino Glacier proved to be unlikely. In any case, better reconstructions and provenance data on the Verbano end-moraine system are needed in order to verify this result.

The Orta chronology in the framework of the Alpine LGM

The Orta morainic amphitheatre provided the largest amount of exposure dates of the Alpine LGM so far. The ages allow us to compare this small lobe to other chronologies known for the Alpine palaeoglaciers (Fig. 8). In the western and northern sectors surface exposure dating results from several studies are available. These include the Reuss (Reber *et al.* 2014), Ivrea (Gianotti *et al.* 2008, 2015) and Rivoli-Avigliana (Ivy-Ochs *et al.* 2018) end-moraine systems and the Maritime Alps (Federici *et al.* 2017). The Orta chronology is in excellent agreement with reports for the Rivoli-Avigliana amphitheatre whose exposure dates were calculated at 24±2 and 19–18 ka for the maximum position and withdrawal phase, respectively.

East of the Orta region, there is the large combined amphitheatre of the Lario-Verbano complex. Radiocarbon dates show that in the Lario amphitheatre the maximum culmination took place before 23 ka; a withdrawal phase started between 22 and 21 ka (Alessio *et al.* 1978; Bini 1997; Scapozza *et al.* 2014). To the east, the Garda (Ravazzi *et al.* 2014; Monegato *et al.* 2017) and Tagliamento (Monegato *et al.* 2007; Fontana *et al.* 2014) amphitheatres show the maximum stand of the glaciers at 26.5–24 ka, followed by a retreat and a re-advance between 23–22 ka, which brought the glacier very close to the earlier maximum position. Considering the presence of several moraines related to the maximum stand of the Orta Glacier, it is likely that a similar twofold scenario took place. The onset of withdrawal after 22 ka has been inferred only through radiocarbon dating in the outwash plain for the Tagliamento (Fontana *et al.* 2014) and the Garda (Monegato *et al.* 2017) systems, with final ice-wastage at about 18–17.5 ka (Ravazzi *et al.* 2014; Rossato & Mozzi 2016; Rossato *et al.* 2018). The second phase at 19 ka recognized in the Orta amphitheatre as a sequence of moraines that can be rightfully ascribed to a glacier stabilization phase. Remarkably, this phase is here chronologically strengthened by five dates directly on the moraines and not through correlation to the outwash deposits as for the Garda (Monegato *et al.* 2017) and the Tagliamento (Fontana *et al.* 2014). Hence, this phase of glacier stabilization can be assumed to have occurred at about 19 ka just before the ice surface lowering in the Alps (Wirsig *et al.* 2016).

Glacier arrival at the maximum position, synchrony or out of phase?

The age assessment of the Orta Glacier being at its maximum before 24 ka is in agreement with those glaciers whose accumulation areas are located close to the fore-Alpine belt like the Tagliamento (Monegato *et al.* 2007) and Oglio (Ravazzi *et al.* 2012) systems. These had short valley reaches, respectively 65 and 75 km long, to fill before arrival on the foreland. The Toce trunk glacier had an overall distance of about 100 km to cover, while the tributary Anza Glacier had a length of about 75 km. According to the available dates, these glaciers could have reached their maximum extents earlier than the largest systems, like the Adige-Sarca at Garda (Monegato *et al.* 2017) or the Rhine (Preusser *et al.* 2011) whose maximum is dated at around 24.5 ka (Fig. 8).

According to some ice-flow models made in the Alps using clast provenance, the inner part of the catchment is always well represented in the spectrum of erratic boulders found in the end-moraine systems (Coutterand *et al.* 2009; Jouvet *et al.* 2017; Cohen *et al.* 2018). In the case of the Orta amphitheatre, the boulders belonging to the Anzasca Valley and to the lower Ossola Valley (Fig. 7) suggest that most of the ice flow can be ascribed to the tributary glacier (Anza Glacier) rather than the major trunk glacier. The rare pebbles that we interpret to stem from the inner Toce catchment are in the eastern sector of the amphitheatre, indicating that during the glaciation contribution from the Toce Glacier did occur mainly along that side.

This provenance signal may be related to the steepness of the Anzasca Valley from the high-elevation accumulation area of the Monte Rosa, which could have led to a high topographic gradient favouring fast ice flow (Fig. 7). In addition, ice accumulation in the Monte Rosa could also have been favoured by high precipitation rates (presently >1800 mm a^{-1}, Isotta *et al.* 2013) with the Monte Rosa being about 45 km far from the Po Plain. Hence, we can infer that the Anza Glacier likely flowed down the lower reach of the Ossola Valley just before the major Toce Glacier, which arrived subsequently to the lower valley and mostly diverted to Lake Maggiore to join the large Ticino glacier to the east.

Considering the waning phase of the glacier, the Orta chronology is more comparable with the Garda system, which was fed by the largest accumulation area on the southern side of the Alps (Monegato *et al.* 2017). The

large and high-elevation accumulation area may have led the glacier to remain in the Orta Valley until the final collapse after 18 ka. From this perspective, local and regional variations, caused by a variety of factors like bed topography, catchment size and elevation, precipitation and temperature, ought to be better understood with the increasing application of numerical flow and climate models to the Alps as one system (Seguinot *et al.* 2018). It is important to be aware of the potentially different responses of adjacent glaciers to the same climate (Kuhn *et al.* 1985).

Conclusions

The Orta end-moraine system consists of closely spaced moraine belts reflecting multiple phases of prolonged glacier stability and subsequent fluvial entrenchments. Previous work shows ambiguous interpretations of the extent of the Orta Glacier during the last glaciation.

Ages obtained through determination of cosmogenic ^{10}Be and ^{36}Cl concentrations in 12 erratic boulders and one bedrock sample show that, contrary to earlier assessments, most of the moraine belts were built up during the LGM. The maximum extent that Orta glacier reached during the LGM is represented by the outer moraine belt. Surface exposure ages of three boulders date this culmination between 26 and 23 ka. About 2 km inwards from these outer moraines, a set of multiple, close-spaced moraines is inferred to reflect a phase of glacier stabilization at about 19 ka just before the beginning of the ice-surface lowering in the Alps. The complete chronology of the Orta Glacier matches with those reported for other glacial amphitheatres on the Italian foreland, which in turn show a perfect fit within the established global glacial maximum between 30 and 19 ka.

The triple-method approach, using (i) boulder lithology, (ii) boulder shape and (iii) glacier flow dynamics, resulted in a reconstruction of the flowlines of the Orta Glacier. It shows that most glacier ice filling the Orta Valley belongs to the eastern Monte Rosa accumulation area, and suggests that this glacier flowing down the Anzasca Valley could have been the trunk glacier spreading into the Orta basin. The closeness of the high elevation accumulation area of the Monte Rosa could have favoured early arrival of the Anza Glacier snout before incursion of the larger Toce Glacier. This suggests that the part played by the location of the accumulation areas should be reconsidered in order to better depict glacier flow along the Alpine valleys.

Acknowledgements. – Funding of fieldwork by the Swiss Quaternary Association (CH-Quat) is greatly appreciated. We thank the Ion Beam Physics group for support of labwork and AMS measurements. We acknowledge A. Ribolini and an anonymous reviewer for the useful comments, which greatly improved the manuscript. We also thank J. A. Piotrowski for his careful suggestions.

Author contributions. – The samples and field data were collected by JB, SI-O, FG and GM; the laboratory preparation and AMS analyses were done by JB and MC; clast petrography identification was done by SM; the manuscript was written and figures prepared by JB, SI-O, GM, FG, SC and SM.

References

Akçar, N., Ivy-Ochs, S., Kubik, P. & Schlüchter, C. 2011: Post-depositional impacts on 'Findlinge' (erratic boulders) and their implications for surface-exposure dating. *Swiss Journal of Geosciences 104*, 445–453.

Alessio, M., Allegri, L., Bella, F., Belluomini, G., Calderoni, G., Cortesi, C., Improta, S., Manfra, L. & Orombelli, G. 1978: I depositi lacustri di Rovagnate, di Pontida e di Pianico in Lombardia: datazione ^{14}C. *Geografia Fisica e Dimanica Quaternaria 1*, 131–137.

Alfimov, V. & Ivy-Ochs, S. 2009: How well do we understand production of ^{36}Cl in limestone and dolomite? *Quaternary Geochronology 4*, 462–474.

André, M. F. 2002: Rates of postglacial rock weathering on glacially scoured outcrops (Abisko–Riksgränsen area, 68 N). *Geografiska Annaler: Series A, Physical Geography 84*, 139–150.

Balco, G., Briner, J., Finkel, R. C., Rayburn, J. A., Ridge, J. C. & Schaefer, J. M. 2009: Regional beryllium-10 production rate calibration for late-glacial northeastern North America. *Quaternary Geochronology 4*, 93–107.

Balco, G., Stone, J. O., Lifton, N. A. & Dunai, T. J. 2008: A complete and easily accessible means of calculating surface exposure ages or erosion rates from ^{10}Be and ^{26}Al measurements. *Quaternary Geochronology 3*, 174–195.

Becker, P., Seguinot, J., Jouvet, G. & Funk, M. 2016: Last Glacial Maximum precipitation pattern in the Alps inferred from glacier modelling. *Geographica Helvetica 71*, 173–187.

Beghin, P., Charbit, S., Dumas, C., Kageyama, M. & Ritz, C. 2015: How might the North American ice sheet influence the northwestern Eurasian climate? *Climate of the Past 11*, 1467–1490.

Benn, D. I. & Ballantyne, C. K. 2005: Palaeoclimatic reconstruction from Loch Lomond Readvance glaciers in the West Drumochter Hills, Scotland. *Journal of Quaternary Science 20*, 577–592.

Benn, D. I. & Evans, D. J. A. 2014: *Glaciers and Glaciations.* 802 pp. Routledge, London.

Benn, D. I., Kirkbride, M. P., Owen, L. A. & Brazier, V. 2003: Glaciated valley landsystems. *In* Evans, D. J. A. (ed.): *Glacial Landsystems*, 372–406. Arnold, London.

Berger, A., Mercolli, I., Kapferer, N. & Fügenschuh, B. 2012: Single and double exhumation of fault blocks in the internal Sesia-Lanzo Zone and the Ivrea-Verbano Zone (Biella, Italy). *International Journal of Earth Sciences 101*, 1877–1894.

Bigioggero, B., Boriani, A., Colombo, A. & Tunesi, A. 1981: Età e caratteri petrochimici degli ortogneiss della zona Moncucco-Orselina nell'area Ossolana. *Rendiconti Societá Italiana di Mineralogia e Petrologia 33*, 207–218.

Bini, A. 1997: Stratigraphy, chronology and paleogeography of Quaternary deposits of the area between the Ticino and Olona rivers (Italy-Switzerland). *Geologia Insubrica 2*, 21–46.

Bini, A., Buoncristiani, J., Couterrand, S., Ellwanger, D., Felber, M., Florineth, D., Graf, H., Keller, O., Kelly, M., Schlüchter, C. & Schoeneich, P. 2009: *Die Schweiz während des letzteiszeitlichen Maximums (LGM)*. Bundesamt für Landestopografie, Wabern.

Bini, A., Bussolini, C., Turri, S. & Zuccoli, L. 2014: Carta geologica alla scala 1:100.000 dell'anfiteatro morenico del Verbano. *Sibrium 28*, 24–81.

Bini, A., Cita, M. B. & Gaetani, M. 1978: Southern Alpine lakes—Hypothesis of an erosional origin related to the Messinian entrenchment. *Marine Geology 27*, 271–288.

Bini, A., Zuccoli, L., Bussolini, C., Corbari, D., Da Rold, O., Ferliga, C., Rossi, S. & Viviani, C. 2004: Glacial history of the southern side of the central Alps, Italy. *Developments in Quaternary Sciences 2*, 195–200.

Borchers, B., Marrero, S., Balco, G., Caffee, M., Goehring, B., Lifton, N., Nishiizumi, K., Phillips, F., Schaefer, J. & Stone, J. 2016:

Geological calibration of spallation production rates in the CRONUS-Earth project. *Quaternary Geochronology 31*, 188–198.
Boriani, A., Origoni, E. G., Borghi, A. & Caironi, V. 1990: The evolution of the "Serie dei Laghi" (Strona-Ceneri and Scisti dei Laghi): the upper component of the Ivrea-Verbano crustal section; Southern Alps, north Italy and Ticino, Switzerland. *Tectonophysics 182*, 103–118.
Boulton, G. S. 1978: Boulder shapes and grain-size distributions of debris as indicators of transport paths through a glacier and till genesis. *Sedimentology 25*, 773–799.
Castiglioni, B. 1940: *L'Italia nell'età quaternaria. Plate No. 3*. Milano, Consociazione Turistica Italiana, Atlante Fisico-economico d'Italia.
Christl, M., Vockenhuber, C., Kubik, P. W., Wacker, L., Lachner, J., Alfimov, V. & Synal, H.-A. 2013: The ETH Zurich AMS facilities: performance parameters and reference materials. *Nuclear Instruments and Methods in Physics Research B 294*, 29–38.
Clark, P. U., Dyke, A. S., Shakun, J. D., Carlson, A. E., Clark, J., Wohlfarth, B., Mitrovica, J. X., Hostetler, S. W. & McCabe, A. M. 2009: The Last Glacial Maximum. *Science 325*, 710–714.
Claude, A., Ivy-Ochs, S., Kober, F., Antognini, M., Salcher, B. & Kubik, P. W. 2014: The Chironico landslide (Valle Leventina, southern Swiss Alps): age and evolution. *Swiss Journal of Geosciences 107*, 273–291.
Cohen, D., Gillet-Chaulet, F., Haeberli, W., Machguth, H. & Fischer, U. H. 2018: Numerical reconstructions of the flow and basal conditions of the Rhine glacier, European Central Alps, at the Last Glacial Maximum. *The Cryosphere 12*, 2515–2544.
Colombi, A. & Pfeifer, H.-R. 1986: Ferrogabbroic and basaltic metaeclogites from the Antrona mafic-ultramafic complex and the Centovalli-Locarno region (Italy and Southern Switzerland) – first results. *Schweizerische Mineralogische und Petrographische Mitteilungen 66*, 99–110.
Compagnoni, R., Dal Piaz, G. V., Hunziker, G. C., Gosso, G., Lombardo, B. & Williams, P. F. 1977: The Sesia-Lanzo Zone, a slice of continental crust with Alpine high pressure—low temperature assemblages in the western Italian Alps. *Rendiconti Societá Italiana di Mineralogia e Petrologia 33*, 281–334.
Coutterand, S., Schoeneich, P. & Nicoud, G. 2009: Le Lobe Glaciaire Lyonnais au maximum würmien glacier du Rhône ou/et glaciers savoyards? *In* Deline P., Ravanel L. (eds.): *Neige et glace de Montagne. Reconstitution, Dynamique, Pratiques*, 11–22. Collection EDYTEM, Cahiers de Géographie, Le Bourget-du-Lac Cedex.
Desilets, D., Zreda, M., Almasi, P. F. & Elmore, D. 2006: Determination of cosmogenic ^{36}Cl in rocks by isotope dilution: innovations, validation and error propagation. *Chemical Geology 233*, 185–195.
Dielforder, A. & Hetzel, R. 2014: The deglaciation history of the Simplon region (southern Swiss Alps) constrained by ^{10}Be exposure dating of ice-molded bedrock surfaces. *Quaternary Science Reviews 84*, 26–38.
Ehlers, J. & Gibbard, P. L. 2004: *Quaternary Glaciations - Extent and Chronology: Part I: Europe*. 488 pp. Elsevier, Amsterdam.
Ernst, W. G. & Dal Piaz, G. V. 1978: Mineral parageneses of eclogitic rocks and related mafic schists of the Piemonte ophiolite nappe, Breuil-St. Jacques area, Italian Western Alps. *American Mineralogist 63*, 621–640.
Evans, J., Stone, J., Fifield, L. & Cresswell, R. 1997: Cosmogenic chlorine-36 production in K-feldspar. *Nuclear Instruments and Methods in Physics Research, Section B 123*, 334–340.
Fairbridge, R. W. 1968: *The Encyclopaedia of Geomorphology*. 1296 pp. Reinhold, New York.
Federici, P. R., Ribolini, A. & Spagnolo, M. 2017: Glacial history of the Maritime Alps from the Last Glacial Maximum to the Little Ice Age. *In* Hughes, P. D. & Woodward, J. C. (eds.): *Quaternary Glaciation in the Mediterranean Mountains*, 137–159. The Geological Society, London.
Felber, M. & Bini, A. 1997: Seismic survey in alpine and prealpine valleys of Ticino (Switzerland): evidences of a Late-Tertiary fluvial origin. *Geologia Insubrica 2*, 46–67.
Ferrando, S., Bernoulli, D. & Compagnoni, R. 2004: The Canavese zone (internal Western Alps): a distal margin of Adria. *Schweizerische Mineralogische und Petrographische Mitteilungen 84*, 237–256.
Finckh, P. G. 1978: Are southern Alpine lakes former Messinian canyons? — Geophysical evidence for preglacial erosion in the southern Alpine lakes. *Marine Geology 27*, 289–302.
Fink, D., Vogt, S. & Hotchkis, M. 2000: Cross-sections for ^{36}Cl from Ti at E_p=35–150 MeV: applications to in situ exposure dating. *Nuclear Instruments and Methods in Physics Research, Section B 172*, 861–866.
Florineth, D. & Schlüchter, C. 1998: Reconstructing the Last Glacial Maximum (LGM) ice surface geometry and flowlines in the Central Swiss Alps. *Eclogae Geologicae Helvetiae 91*, 391–407.
Fontana, A., Monegato, G., Zavagno, E., Devoto, S., Burla, I. & Cucchi, F. 2014: Evolution of an Alpine fluvioglacial system at the LGM decay: the Cormor megafan (NE Italy). *Geomorphology 204*, 136–153.
Forno, M. G., Gianotti, F. & Racca, G. 2010: Significato paleoclimatico dei rapporti tra il glacialismo principale e quello tributario nella bassa Valle della Dora Baltea. *Il Quaternario - Italian Journal of Quaternary Sciences 23*, 105–124.
Frey, M., Desmons, J. & Neubauer, F. 1999: The new metamorphic map of the Alps. *Schweizerische Mineralogische und Petrographische Mitteilungen 79*, 1–4.
Frey, M., Hunziker, J. C., Frank, W., Bocquet, J., Dal Piaz, G. V., Jäger, E. & Niggli, E. 1974: Alpine metamorphism of the Alps. A review. *Schweizerische Mineralogische und Petrographische Mitteilungen 54*, 247–290.
Gianotti, F., Forno, M. G., Ivy-Ochs, S. & Kubik, P. W. 2008: New chronological and stratigraphical data on the Ivrea amphitheatre (Piedmont, NW Italy). *Quaternary International 190*, 123–135.
Gianotti, F., Forno, M. G., Ivy-Ochs, S., Monegato, G., Pini, R. & Ravazzi, C. 2015: Stratigraphy of the Ivrea Morainic Amphitheatre (NW Italy): an updated synthesis. *Alpine and Mediterranean Quaternary 28*, 29–58.
Guyot, A. 1847: Note sur la distribution des especes de roches dans le bassin erratique du Rhône. *Bulletin de la Société des Sciences Naturelles de Neuchâtel 1*, 477–506.
Hantke, R. 1983: *Eiszeitalter. Westliche Ostalpen mit ihrem bayerischen Vorland bis zum Inn-Durchbruch und Südalpen zwischen Dolomiten und Mont Blanc*. 730 pp. Ott Verlag, Thun.
Heiri, O., Koinig, K. A., Spötl, C., Barrett, S., Brauer, A., Drescher-Schneider, R., Gaar, D., Ivy-Ochs, S., Kerschner, H., Luetscher, M., Moran, A., Nicolussi, K., Preusser, F., Schmidt, R., Schoeneich, P., Schwörer, C., Sprafke, T., Terhorst, B. & Tinner, W. 2014: Palaeoclimate records 60–8 ka in the Austrian and Swiss Alps and their forelands. *Quaternary Science Reviews 106*, 186–205.
Isotta, F. A., Frei, C., Weilguni, V., Tadi′c, M. P., Lassègues, P., Rudolf, B., Pavan, V., Cacciamani, C., Antolini, G., Ratto, S. M., Munari, M., Micheletti, S., Bonati, V., Lussana, C., Ronchi, C., Panettieri, E., Marigo, G. & Vertačnik, G. 2013: The climate of daily precipitation in the Alps: development and analysis of a high resolution grid dataset from pan-Alpine rain-gauge data. *International Journal of Climatology 34*, 1657–1675.
Ivy-Ochs, S. 1996: *The dating of rock surfaces using in situ produced ^{10}Be, ^{26}Al and ^{36}Cl, with examples from Antarctica and the Swiss Alps*. Ph.D. thesis, ETH Zürich, 196 pp.
Ivy-Ochs, S. 2015: Glacier variations in the European Alps at the end of the last glaciation. *Cuadernos de Investigación Geográfica 41*, 295–315.
Ivy-Ochs, S. & Kober, F. 2008: Surface exposure dating with cosmogenic nuclides. *E&G Quaternary Science Journal 57*, 179–209.
Ivy-Ochs, S., Kerschner, H., Reuther, A., Preusser, F., Heine, K., Maisch, M., Kubik, P. W. & Schlüchter, C. 2008: Chronology of the last glacial cycle in the European Alps. *Journal of Quaternary Science 23*, 559–573.
Ivy-Ochs, S., Lucchesi, S., Baggio, P., Fioraso, G., Gianotti, F., Monegato, G., Graf, A. A., Akçar, N., Christl, M., Carraro, F., Forno, M. G. & Schlüchter, C. 2018: New geomorphological and chronological constraints for glacial deposits in the Rivoli-Avigliana end-moraine system and the lower Susa Valley (Western Alps, NW Italy). *Journal of Quaternary Science 33*, 550–562.
Ivy-Ochs, S., Schäfer, J., Kubik, P. W., Synal, H.-A. & Schlüchter, C. 2004a: Timing of deglaciation on the northern Alpine foreland (Switzerland). *Eclogae Geologicae Helvetiae 97*, 47–55.

Ivy-Ochs, S., Synal, H. A., Roth, C. & Schaller, M. 2004b: Initial results from isotope dilution for Cl and ^{36}Cl measurements at the PSI/ETH Zurich AMS facility. *Nuclear Instruments and Methods in Physics Research, Section B 223–224*, 623–627.

Jäckli, H. 1970: *Die Schweiz zur letzten Eiszeit. Atlas der Schweiz (1: 550 000). Blatt 6.* Verlag Eidgenössische Landestopographie, Bern.

Jorda, M., Rosique, T. & Evin, J. 2000: Donnéees nouvelles sur l'age du dernier maximum glaciaire dans les Alpes méridionales françaises. *Comptes Rendus de l'Académie des Sciences - Series IIA - Earth and Planetary Science 331*, 187–193.

Jouvet, G., Seguinot, J., Ivy-Ochs, S. & Funk, M. 2017: Modelling the diversion of erratic boulders by the Valais Glacier during the last glacial maximum. *Journal of Glaciology 63*, 487–498.

Keller, L. M., Hess, M., Fügenschuh, B. & Schmid, S. M. 2005: Structural and metamorphic evolution of the Camughera-Moncucco, Antrona and Monte Rosa units southwest of the Simplon line, western Alps. *Eclogae Geologicae Helvetiae 98*, 19–49.

Kelly, M. A., Buoncristiani, J.-F. & Schlüchter, C. 2004: A reconstruction of the last glacial maximum (LGM) ice-surface geometry in the western Swiss Alps and contiguous Alpine regions in Italy and France. *Eclogae Geologicae Helvetiae 97*, 57–75.

Kohl, C. & Nishiizumi, K. 1992: Chemical isolation of quartz for measurement of in-situ-produced cosmogenic nuclides. *Geochimica et Cosmochimica Acta 56*, 3583–3587.

Kuhlemann, J., Rohling, E., Krumrei, I., Kubik, P., Ivy-Ochs, S. & Kucera, M. 2008: Regional synthesis of Mediterranean atmospheric circulation during the last glacial maximum. *Science 321*, 1338–1340.

Kuhn, M., Markl, G., Kaser, G., Nickus, U., Obleitner, F. & Schneider, H. 1985: Fluctuations of climate and mass balance: different responses of two adjacent glaciers. *Zeitschrift für Gletscherkunde und Glazialgeologie 21*, 409–416.

Lal, D. 1991: Cosmic ray labeling of erosion surfaces: in situ nuclide production rates and erosion models. *Earth and Planetary Science Letters 104*, 424–439.

Lambeck, K., Rouby, H., Purcell, A., Sun, Y. & Sambridge, M. 2014: Sea level and global ice volumes from the last glacial maximum to the Holocene. *Proceedings of the National Academy of Sciences of the United States of America 111*, 15296–15303.

Larson, P. C. & Mooers, H. D. 2004: Glacial indicator dispersal processes: a conceptual model. *Boreas 33*, 238–249.

Luetscher, M., Boch, R., Sodemann, H., Spötl, C., Cheng, H., Edwards, R. L., Frisia, S., Hof, F. & Müller, W. 2015: North Atlantic storm track changes during the last glacial maximum recorded by alpine speleothems. *Nature Communications 6*, 6344, https://doi.org/10.1038/ncomms7344.

Lukas, S., Benn, D. I., Boston, C. M., Brook, M., Coray, S., Evans, D. J. A., Graf, A., Kellerer-Pirklbauer, A., Kirkbride, M. P., Krabbendam, M., Lovell, H., Machiedo, M., Mills, S. C., Nye, K., Reinardy, B. T. I., Ross, F. H. & Signer, M. 2013: Clast shape analysis and clast transport paths in glacial environments: a critical review of methods and the role of lithology. *Earth-Science Reviews 121*, 96–116.

Mandier, P., Evin, J., Argant, J. & Petiot, R. 2003: Chronostratigraphie des accumulations würmiennes dans la moyenne vallée du Rhône. L'apport des dates radiocarbon. *14*, 113–127.

Marrero, S. M., Phillips, F. M., Caffee, M. W. & Gosse, J. C. 2016: CRONUS-Earth cosmogenic ^{36}Cl calibration. *Quaternary Geochronology 31*, 199–219.

Menzies, J. 2003: Tills and tillites. *In* Middleton, G. (ed.): *Encyclopedia of Sediments and Sedimentary Rocks*, 744–747. Kluwer Academic Publishers, Boston.

Monegato, G. & Ravazzi, C. 2018: The late Pleistocene multifold glaciation in the Alps: updates and open questions. *Alpine and Mediterranean Quaternary 31*, 225–229.

Monegato, G., Ravazzi, C., Donegana, M., Pini, R., Calderoni, G. & Wick, L. 2007: Evidence of a two-fold glacial advance during the last glacial maximum in the Tagliamento end moraine system (eastern Alps). *Quaternary Research 68*, 284–302.

Monegato, G., Scardia, G., Hajdas, I., Rizzini, F. & Piccin, A. 2017: The Alpine LGM in the boreal ice-sheets game. *Scientific Reports 7*, 2078, https://doi.org/10.1038/s41598-017-02148-7.

Naughton, F., Sámchez-Goñi, M. F., Kageyama, M., Bard, E., Dupart, J., Cortijo, E., Despart, S., Malaizé, B., Joly, C., Rostek, F. & Turon, J.-L. 2009: Wet to dry climatic trend in north-western Iberia within Heinrich events. *Earth Planetary Science Letters 284*, 329–342.

Nishiizumi, K., Imamura, M., Caffee, M. W., Southon, J. R., Finkel, R. C. & McAninch, J. 2007: Absolute calibration of ^{10}Be AMS standards. *Nuclear Instruments and Methods in Physics Research, Section B 258*, 403–413.

Novarese, V. 1927: Gli apparati morenici würmiani del Lago Maggiore e del Lago d'Orta. *Bollettino dell'Ufficio Geologico Italiano 8*, 1–64.

Oberhänsli, R., Bousquet, R., Engi, M., Goffé, B., Gosso, G., Handy, M., Häck, V., Koller, F., Lardeaux, J. M., Polino, R., Rossi, P., Schuster, R., Schwartz, S. & Spalla, M. I. 2004: *Metamorphic Structure of the Alps.* Commission of the Geological Map Wo, Paris.

Pellegrini, G. B., Albanese, D., Bertoldi, R. & Surian, N. 2005: La deglaciazione alpina nel Vallone Bellunese, Alpi meridionali orientali. *Supplementi Geografia Fisica e Dinamica Quaternaria 7*, 271–280.

Penck, A. & Brückner, E. 1901–1909: *Die Alpen im Eiszeitalter.* 1199 pp. Tauchnitz, Leipzig.

Pfiffner, O. A., Lehner, P., Heitzmann, P., Mueller, S. & Steck, A. 1997: *Deep Structure of the Swiss Alps: Results of NRP 20*. 460 pp. Birkhäuser Verlag, Basel.

Piana, F., Fioraso, G., Irace, A., Mosca, P., d'Atri, A., Barale, L., Falletti, P., Monegato, G., Morelli, M., Tallone, S. & Vigna, G. B. 2017: Geology of Piemonte region (NW Italy, Alps-Apennines interference zone). *Journal of Maps 13*, 395–405.

Pinarelli, L., Boriani, A. & Del Moro, A. 1993: The Pb isotopic systematics during crustal contamination of subcrustal magmas: the Hercynian magmatism in the Serie dei Laghi (Southern Alps, Italy). *Lithos 31*, 51–61.

Preusser, F. 2004: Towards a chronology of the Late Pleistocene in the northern Alpine Foreland. *Boreas 33*, 195–210.

Preusser, F., Graf, H. R., Keller, O., Krayss, E. & Schlüchter, C. 2011: Quaternary glaciation history of northern Switzerland. *E&G Quaternary Science Journal 60*, 282–305.

Ravazzi, C., Badino, F., Marsetti, D., Patera, G. & Reimer, P. J. 2012: Glacial to paraglacial history and forest recovery in the Oglio glacier system (Italian Alps) between 26 and 15 ka cal BP. *Quaternary Science Reviews 58*, 146–161.

Ravazzi, C., Pini, R., Badino, F., De Amicis, M., Londeix, L. & Reimer, P. J. 2014: The latest LGM culmination of the Garda Glacier (Italian Alps) and the onset of glacial termination. Age of glacial collapse and vegetation chronosequence. *Quaternary Science Reviews 105*, 26–47.

Reber, R., Akçar, N., Ivy-Ochs, S., Tikhomirov, D., Burkhalter, R., Zahno, C., Lüthold, A., Kubik, P. W., Vockenhuber, C. & Schlüchter, C. 2014: Timing of retreat of the Reuss glacier (Switzerland) at the end of the last glacial maximum. *Swiss Journal of Geosciences 107*, 293–307.

Reinhardt, B. 1966: Geologie und Petrographie der Monte Rosa-Zone, der Sesia-Zone und des Canavese im Gebiet zwischen Valle d'Ossola und Valle Loana (Prov. Novara, Italien). *Schweizerische Mineralogische und Petrographische Mitteilungen 46*, 553–678.

Reitner, J. R., Ivy-Ochs, S., Drescher-Schneider, R., Hajdas, I. & Linner, M. 2016: Reconsidering the current stratigraphy of the Alpine Lateglacial: implications of the sedimentary and morphological record of the Lienz area (Tyrol/Austria). *E&G Quaternary Science Journal 65*, 113–144.

Rossato, S. & Mozzi, P. 2016: Inferring LGM sedimentary and climatic changes in the southern Eastern Alps foreland through the analysis of a ^{14}C ages database (Brenta megafan, Italy). *Quaternary Science Reviews 148*, 115–127.

Rossato, S., Carraro, A., Monegato, G., Mozzi, P. & Tateo, F. 2018: Glacial dynamics in pre-Alpine narrow valleys during the Last Glacial Maximum inferred by lowland fluvial records (northeast Italy). *Earth Surface Dynamics 6*, 809–828.

Rutter, E., Brodie, K., James, T. & Burlini, L. 2007: Large-scale folding in the upper part of the Ivrea-Verbano zone, NW Italy. *Journal of Structural Geology 29*, 1–17.

Sacco, F. 1930: Il Glacialismo nelle Valli Sesia: Strona, Anza e nell'Ossola. *Ufficio idrografico del Po Pubblicazione 4/10*, 35–69.

Salcher, B. C., Starnberger, R. & Götz, J. 2015: The last and penultimate glaciation in the North Alpine Foreland: new stratigraphical and

chronological data from the Salzach glacier. *Quaternary International 388*, 218–231.
Scapozza, C., Castelletti, C., Soma, L., Dall'Agnolo, S. & Ambrosi, C. 2014: Timing of LGM and deglaciation in the Southern Swiss Alps. *Géomorphologie: Relief, Processus, Environnement 4*, 307–322.
Seguinot, J., Ivy-Ochs, S., Jouvet, G., Huss, M., Funk, M. & Preusser, F. 2018: Modelling last glacial cycle ice dynamics in the Alps. *Cryosphere 12*, 3265–3285.
Stone, J. O. 2000: Air pressure and cosmogenic isotope production. *Journal of Geophysical Research: Solid Earth 105(B10)*, 23753–23759.
Stone, J. O., Allan, G. L., Fifield, L. K. & Cresswell, R. G. 1996: Cosmogenic chlorine-36 from calcium spallation. *Geochimica et Cosmochimica Acta 60*, 679–692.
Stone, J. O. H., Evans, J. M., Fifield, L. K., Allan, G. L. & Cresswell, R. G. 1998: Cosmogenic chlorine-36 production in calcite by muons. *Geochimica et Cosmochimica Acta 62*, 433–454.
Stone, J. O., Fifield, K. & Vasconcelos, P. 2005: Terrestrial chlorine-36 production from spallation of iron. Abstract of 10th International Conference on Accelerator Mass Spectrometry. Berkeley, California.
Svensson, A., Andersen, K. K., Bigler, M., Clausen, H. B., Dahl-Jensen, D., Davies, S. M., Johnsen, S. J., Muscheler, R., Rasmussen, S. O., Röthlisberger, R., Steffensen, J. P. & Vinther, B. M. 2006: The Greenland ice core chronology 2005, 15-42 ka. Part 2: comparison to other records. *Quaternary Science Reviews 25*, 3258–3267.
Swisstopo 2005: *Geological Map of Switzerland, 1:500,000*. Swiss Federal Office of Topography, Wabern.
Synal, H. A., Bonani, G., Döbeli, M., Ender, R. M., Gartenmann, P., Kubik, P. W., Schnabel, C. & Suter, M. 1997: Status report of the PSI/ETH AMS facility. *Nuclear Instruments and Methods in Physics Research, Section B 123*, 62–68.
Turco, F. & Tartarotti, P. 2006: The Antrona Nappe: lithostratigraphy and metamorphic evolution of ophiolites in the Antrona Valley (Pennine Alps). *Ofioliti 31*, 207–221.
Vai, G. B. & Cantelli, L. 2004: *Litho-Palaeoenvironmental Maps of Italy During the Last Two Climatic Extremes. Two Maps 1:1,000,000*. LAC, Firenze.
Vockenhuber, C., Miltenberger, K. U. & Synal, H. A. 2019: ^{36}Cl measurements with a gas-filled magnet at 6 MV. *Nuclear Instruments and Methods in Physics Research, Section B 455*, 190–194.
Wirsig, C., Zasadni, J., Christl, M., Akçar, N. & Ivy-Ochs, S. 2016: Dating the onset of LGM ice surface lowering in the High Alps. *Quaternary Science Reviews 143*, 37–50.

Supporting Information

Additional Supporting Information may be found in the online version of this article at http://www.boreas.dk.

Table S1. Elemental composition of rock samples dated with cosmogenic ^{36}Cl.